Numerical investigation of wave steepening and shock coalescence near a cold Mach 3 jet

Pierre Pineau, Christophe Bogey

JASA INVITED-PAPER

Numerical investigation of wave steepening and shock coalescence near a cold Mach 3 jet[a)]

Pierre Pineau[b)] and Christophe Bogey[c)]
Univ. Lyon, École Centrale de Lyon, INSA Lyon, Université Claude Bernard Lyon I, CNRS, Laboratoire de Mécanique des Fluides et d'Acoustique, UMR 5509, F-69134 Ecully, France

ABSTRACT:
Wave steepening and shock coalescence due to nonlinear propagation effects are investigated for a cold Mach 3 jet. The jet flow and near pressure fields are computed using large-eddy simulation. The near acoustic field is propagated to the far field by solving the linearized or the weakly nonlinear Euler equations. Near the angle of peak levels, the skewness factors of the pressure fluctuations for linear and nonlinear propagations display positive values that are almost identical. Thus, the positive asymmetry of the fluctuations originates during the wave generation process and is not due to nonlinear propagation effects. Compressions in the signals are much steeper for a nonlinear than for a linear propagation, highlighting the crucial role of nonlinear distortions in the formation of steepened waves. The power transfers due to nonlinear propagation are examined for specific frequencies by considering the spatial distribution of the Morfey–Howell indicator in the near and far acoustic fields. They are in good agreement with the direct measurements performed by comparing the spectra for nonlinear and linear propagations. This shows the suitability of the Morfey–Howell indicator to characterize nonlinear distortions for supersonic jets.
 https://doi.org/10.1121/10.0003343
(Received 2 July 2020; revised 20 December 2020; accepted 22 December 2020; published online 14 January 2021)
[Editor: Kent L. Gee] Pages: 357–370

I. INTRODUCTION

Propagation of acoustic waves generated by high-speed jets is usually modeled as a linear phenomenon, since the amplitude of the acoustic fluctuations is low with respect to the ambient pressure. While this assumption holds for subsonic and moderately supersonic jets, it has been shown to be disputable in the case of highly supersonic jets such as those powering military jet fighters and rocket launchers (Crighton and Bashforth, 1980; Gee *et al.*, 2008; McInerny and Ölçmen, 2005; Morfey and Howell, 1981; Schlinker *et al.*, 2007). For instance, by analyzing the noise radiated by high-performance aircrafts over long propagation distances, Morfey and Howell (1981) observed an excess of high-frequency noise with respect to predictions based on linear models. This noise excess was attributed to nonlinear distortions caused by the intense pressure levels, which can exceed 140 dB at 20 m from a jet engine at full power (Gee *et al.*, 2008; Morfey and Howell, 1981). Accurately predicting the acoustic waves produced by high-speed supersonic jets requires taking into account these nonlinear distortions as they can have a significant impact on the acoustic field. Notably, nonlinear propagation effects are expected to play a key role in the formation of crackle noise (Ffowcs Williams *et al.*, 1975), which is an unpleasant perception effect attributed to the rapid succession of sharp compressions and gradual expansions in acoustic pressure signals (Gee *et al.*, 2018a; Tam *et al.*, 2018). Indeed, when propagation is nonlinear, strong positive peaks propagate faster than the other components in the signals, leading to the formation of shocks and to a nonlinear power transfer from middle to high frequencies as revealed by experimental measurements (Fiévet *et al.*, 2016; Gallagher and McLaughlin, 1981; Gee *et al.*, 2008; Petitjean *et al.*, 2006) and numerical simulations (de Cacqueray and Bogey, 2014; Saxena *et al.*, 2009; Shepherd *et al.*, 2009) of the nonlinear propagation of jet noise. Moreover, nonlinear propagation effects can cause these shocks to coalesce, leading to fewer of them for longer propagation distances, which is also observed in some of the aforementioned studies (Fiévet *et al.*, 2016; Gallagher and McLaughlin, 1981; Saxena *et al.*, 2009; Shepherd *et al.*, 2009).

It has, however, been argued that nonlinear propagation effects are not the only mechanism involved in the formation of the steepened waves at the origin of crackle. This is particularly true for jets exiting from small-scale nozzles such as those considered in most experiments. For these jets, the peak frequencies are higher than in full-scale jet engines so that the effects of molecular absorption are stronger and can counteract those of nonlinear propagation. By combining detailed sound measurements in the acoustic field of a cold Mach 3 jet of diameter 2.5 cm and a wavepacket model for the source, Fiévet *et al.* (2016) and Baars *et al.* (2016) suggested that nonlinear propagation effects dominate those of the molecular absorption in the jet near field, where sound intensity decays according to a cylindrical law, but that they

[a)]This paper is part of a special issue on Supersonic Jet Noise.
[b)]Electronic mail: pierre.pineau@ec-lyon.fr, ORCID: 0000-0002-1251-109X.
[c)]ORCID: 0000-0003-3243-747X.

are almost nonexistent in the far acoustic field, where sound intensity decays following a spherical law. Based on the estimation of the propagation distances required for shock formation, they concluded that nonlinear propagation effects, alone, were not sufficient to explain the presence of shocks in the far-field pressure signal. Moreover, other authors (Ffowcs Williams *et al.*, 1975; Krothapalli *et al.*, 2000; Lighthill, 1994) suggested that shock formation can occur at the source, inside the turbulent flow, which is visible in optical visualizations (Krothapalli *et al.*, 2000; Lowson and Ollerhead, 1968; Murray and Lyons, 2016; Papamoschou, 1995; Rossmann *et al.*, 2002) and numerical simulations (Buchta and Freund, 2017; Nichols *et al.*, 2013; Pineau and Bogey, 2019, 2020) showing the presence of shocks embedded inside the turbulent flow for supersonic jets and free-shear flows. These steepened waves, which are too close from the jet to result from nonlinear propagation effects alone, then propagate to the far field, leading to shock structures possessing the distinctive features of crackle. The formation of these waves has recently received much attention, since a better understanding of the mechanisms involved could allow us to mitigate crackle using noise reduction devices acting on the jet flow such as microjets (Krothapalli *et al.*, 2002), chevrons (Martens *et al.*, 2011), or nozzle inserts (Murray and Lyons, 2016). In particular, using conditional averages, the generation of steepened Mach waves was related by the authors of the present paper (Pineau and Bogey, 2018, 2019, 2020) to the supersonic convection of large-scale coherent structures in the jet shear layers. These coherent structures act on the surrounding medium as supersonically traveling bluff bodies or wavy walls and generate positively skewed, steepened waveforms (Buchta and Freund, 2019).

The respective roles of nonlinear propagation effects and source steepening in the formation of crackle are difficult to distinguish. This is due, in large part, to the lack of a unique, unambiguous definition of this perception effect. In the past, several statistical indicators have been introduced (Baars and Tinney, 2014; Ffowcs Williams *et al.*, 1975; Fiévet *et al.*, 2016; Gallagher and McLaughlin, 1981; McInerny, 1996; Mora *et al.*, 2014), most of them measuring a particular aspect of the pressure fluctuation signals presumably linked to crackle. Among these indicators, which include the skewness and kurtosis factors of the pressure fluctuations, the skewness and kurtosis factors of the pressure time derivative, or the wave-steepening factor (WSF), only the skewness factor of the pressure time derivative has been directly related to the perception of crackle through listening tests (Gee *et al.*, 2018a). In addition, while some of them, such as the skewness factor of the pressure time derivative, or the WSF, significantly increase with the distance from the jet (Fiévet *et al.*, 2016; Gallagher and McLaughlin, 1981; Gee *et al.*, 2013; Petitjean *et al.*, 2006), suggesting nonlinear propagation effects, some others, such as the skewness factor of the pressure fluctuations, appear to be relatively insensitive to the propagation distance (Buchta and Freund, 2017; Mora *et al.*, 2014). Depending on the indicator considered, this has led to inconsistent conclusions on whether crackle is mostly a nonlinear propagation effect or the consequence of a source mechanism.

Another challenge in the study of nonlinear propagation effects is that the sources of supersonic jet noise are distributed over a large extent of the jet flow, which complicates any assessment of nonlinear propagation effects based on a single linear array of microphones. According to Fiévet *et al.* (2016), who measured pressure signals at different locations on a linear array of microphones originating from the end of the potential core, the acoustic waves produced by the jet can be considered as spherical for propagation distances greater than $40D$. The minimum distance can even be as long as $70D$ when the microphone array originates from the nozzle exit (Fiévet *et al.*, 2016; Kuo *et al.*, 2012). This is unfortunate, as nonlinear propagation effects are expected to be strongest near the jet, where the pressure levels are highest.

Finally, molecular relaxation and thermoviscous effects can also gradually change the waveforms as the propagation distance increases. This linear phenomenon mostly affects the high-frequency components of the signals, which are also those that are the most strongly influenced by nonlinear propagation effects. The respective roles of nonlinear propagation effects and molecular absorption can be assessed by computing the Gol'dberg number, which is a dimensionless parameter defined as the ratio between the length scales associated with nonlinear propagation and molecular absorption, respectively. In the experiments of the literature, this parameter can vary over several orders of magnitude when the effects of spherical spreading are accounted for (Hamilton, 2016), even for jets with very similar Mach numbers and temperatures, as illustrated by Baars *et al.* (2016). It is argued that these differences can explain some of the inconsistencies reported in the literature regarding the role of nonlinear propagation effects in supersonic jet noise.

A direct way to assess the effects of nonlinear propagation on supersonic jet noise is to compare the linear and nonlinear propagation of a given signal using time domain simulations. In this way, the changes in the crackle indicators imputable to nonlinear propagation effects can be isolated. This has been done, for instance, by Gee *et al.* (2008) and Saxena *et al.* (2009) using a generalized Burgers equation and by Shepherd *et al.* (2009) by solving the one-dimensional Navier–Stokes equations. These studies, however, rely on one-dimensional models, which cannot take into account the spatial distribution of the sound sources in supersonic jets. In particular, it has been suggested (Fiévet *et al.*, 2016) that nonlinear interactions between waves emitted from different locations in the jet flow play an important role in the steepening of the waves associated with crackle. Full, three-dimensional simulations of the nonlinear propagation of jet noise reproduce these interactions, but they are, unfortunately, rare due to their high computational cost. Such studies have been performed, for instance, by de Cacqueray and Bogey (2014) and Langenais *et al.* (2019), who propagated to the far field the near field pressure fluctuations obtained from a large-eddy simulation (LES) by solving the linear and full nonlinear Euler equations.

https://doi.org/10.1121/10.0003343

In the present study, the formation of steepened waves in the sound field of a cold Mach 3 jet is studied using numerical simulations. The jet exhaust conditions are very close to those in the experiments carried out at the University of Texas at Austin (Baars *et al.*, 2014; Baars and Tinney, 2014; Fiévet *et al.*, 2016). The jet flow and very-near acoustic fields are computed using high-fidelity LES, and the far acoustic fields are extrapolated from the LES pressure fields by solving the linear and weakly nonlinear Euler equations (Gloerfelt *et al.*, 2003). The mesh grids used for the LES and the acoustic propagation are carefully designed to simulate the propagation of high-frequency waves for which nonlinear effects are strongest. Indeed, the combination of high-order schemes and fine grids allows us to accurately resolve these waves up to a Strouhal number of $St = fD/u_j = 5$. This is significantly higher than the cutoff Strouhal numbers of 0.3 and 1 in the simulations of Langenais *et al.* (2019) and de Cacqueray and Bogey (2014), respectively, as well as that in the experiments of Baars and co-workers (Baars *et al.*, 2014; Baars and Tinney, 2014; Baars *et al.*, 2016), in which the maximum Strouhal number is close to 2. The linear propagation allows us to reveal the properties of the acoustic field without nonlinear propagation effects outside of the LES domain, thus highlighting the contribution of the source steepening mechanism to the formation of the steepened waves at the origin of crackle. Then the effects of nonlinear distortions can be identified by comparing the nonlinearly and linearly propagated signals. Since crackle is a perception effect, assessing its presence requires careful listening tests, such as the ones performed in Gee *et al.* (2018a). This was not possible in the present study due to the short duration of the signals. Instead, classical nonlinearity indicators, including the WSF, the zero-crossing rate (ZCR), and the skewness factors of the pressure fluctuations and of their time derivative, are computed to identify wave steepening and shock coalescence in the jet near and far acoustic fields. The main objective is to identify which of these indicators are affected by nonlinear propagation effects and how. Finally, nonlinear exchanges of power resulting from these distortions are also characterized. In particular, the flux of power transfers is analyzed by considering the Morfey–Howell nonlinearity indicator (Morfey and Howell, 1981), and changes in the spectra are determined by comparing the power spectrum densities (PSDs) for linear and nonlinear propagations.

The paper is organised as follows. First, the LES methodology is described, and the linear and nonlinear propagation methods are introduced in Sec. II. The results are presented in Sec. III. They include several crackle indicators, pressure signals, and spectra at different locations, as well as the spatial distribution of the Morfey–Howell nonlinearity indicator. Finally, concluding remarks are given in Sec. IV.

II. NUMERICAL METHODOLOGY

A. Jet parameters

The jet conditions considered in the present study are very similar to those in the experiments of Baars *et al.* (2014) and Fiévet *et al.* (2016). The jet is perfectly expanded and exits from a straight-pipe nozzle at a Mach number $M_j = u_j/a_j$ of 3, where u_j is the exit velocity and $a_j = \sqrt{\gamma r T_j}$ is the speed of sound at the nozzle exit, with $\gamma = 1.4$ the ratio of specific heat, r the ideal gas constant, and T_j the static temperature. The stagnation temperature T_s is equal to T_∞, where $T_\infty = 293\,\mathrm{K}$ is the ambient temperature, which yields an acoustic Mach number $M_a = u_j/a_\infty = 1.77$, where a_∞ is the speed of sound in the ambient medium. The diameter-based Reynolds number $Re_D = u_j D/\nu_j$ of the jet is equal to 2×10^5, where $D = 2r_0 = 0.7$ mm is the jet diameter and ν_j is the kinematic viscosity computed from the Sutherland's law. It is lower than the Reynolds number considered in the above experiments, which is of $Re_D = 7.2 \times 10^6$, to limit the computational cost of the simulations. In the nozzle, a Blasius-like velocity profile of thickness $\delta_{BL} = 0.15 r_0$ is prescribed, and random vortical disturbances are added in the boundary layers to favor the transition of the mixing layer from a laminar to a turbulent state. These disturbances are Gaussian vortex rings of random phases and amplitudes, as proposed in Bogey *et al.* (2011b). Their mean amplitude has been tuned to yield peak turbulence rates of 3% at the nozzle exit so that the jet shear layers are initially in a weakly disturbed state.

B. LES methodology

The LES is carried out by solving the filtered compressible Navier–Stokes equations in cylindrical coordinates (r, θ, z) using high-order schemes. The spatial derivatives are evaluated using centered, fourth-order, 11-point finite differences, and a six-stage Runge–Kutta algorithm is used for time integration (Bogey and Bailly, 2004). Near the jet axis, the method of Mohseni and Colonius (2000) is used to treat the singularity at $r = 0$, and the derivatives are computed using fewer points than permitted by the grid to relieve the time step constraint due to the use of explicit schemes (Bogey *et al.*, 2011a). At the end of each time step, a sixth-order selective filter (Bogey *et al.*, 2009) is applied to damp grid-to-grid oscillations. This filter also serves as an implicit subgrid scale model relaxing turbulent kinetic energy near the grid cutoff wavenumber (Bogey and Bailly, 2006, 2009). A shock capturing adaptive filtering (Bogey and Bailly, 2009) is also applied to remove Gibbs oscillations that are formed near shocks. Finally, non-reflecting radiation boundary conditions (Bogey and Bailly, 2002; Tam and Dong, 1996) are prescribed at the inflow, outflow, and radial limits of the computational domain.

The LES computational domain extends down to $z = 35D$ in the axial direction and out to $r = 9D$ in the radial direction. It contains a total number of $n_r \times n_\theta \times n_z = 511 \times 256 \times 2481 = 325 \times 10^6$ points. Since the objective of the present simulation is to investigate the generation of steepened acoustic waves near the jet, specific care has been taken to accurately resolve high-frequency components in the near acoustic field. In particular, the axial and radial mesh spacings Δz and Δr do not exceed $0.025D$, which

yields a maximum Strouhal number $St = f_{max}D/u_j$ of 5, where f_{max} is the maximum frequency for an acoustic wave discretized using four points per wavelength. After an initial transient period, the flow and sound field are recorded during a time of $1100D/u_j$. In particular, the flow variables are recorded at a sampling Strouhal number of $f_sD/u_j = 5$, where $f_s = 17.4$ MHz is the sampling frequency, on a closed cylindrical surface at $r = 7.5D$ from the jet axis, spanning the whole axial extent of the computational domain, from the inflow at $z = -0.75D$ down to the outflow at $z = 35D$.

C. Wave extrapolation methods

The linear and nonlinear extrapolations are carried out by solving the set of Eq. (1) in cylindrical coordinates, where u'_r, u'_θ and u'_z are the radial, azimuthal, and axial components of the fluctuating velocity, and $p' = p - p_\infty$ is the acoustic pressure,

$$\begin{aligned}
&\frac{\partial u'_r}{\partial t} + \frac{1}{\rho_\infty}\frac{\partial p'}{\partial r} = 0,\\
&\frac{\partial u'_\theta}{\partial t} + \frac{1}{\rho_\infty}\frac{1}{r}\frac{\partial p'}{\partial \theta} = 0,\\
&\frac{\partial u'_z}{\partial t} + \frac{1}{\rho_\infty}\frac{\partial p'}{\partial z} = 0,\\
&\frac{\partial p'}{\partial t} + \rho_\infty a^2\left(\frac{\partial u'_r}{\partial r} + \frac{1}{r}\frac{\partial u'_\theta}{\partial \theta} + \frac{\partial u'_z}{\partial z}\right) = 0.
\end{aligned} \tag{1}$$

The first three equations are the linearized, lossless momentum equations, and the last one is a continuity equation combined with the isentropic equation of state. For linear propagation, the speed of sound a is constant and equal to a_∞ so that the linear extrapolation is performed by solving the linearized Euler equations. For a nonlinear propagation, however, the speed of sound depends on the local value of the pressure fluctuations. For moderately weak pressure perturbations, it can be estimated using the following first order modification (Whitham, 1974),

$$a = a_\infty\left(1 + \frac{\gamma+1}{2\gamma}\frac{p'}{p_\infty}\right). \tag{2}$$

Including expression (2) for the speed of sound in Eq. (1) allows us to take into account nonlinear propagation effects in the weak shock limit at a moderate cost. Notably, this approach is consistent with second-order, lossless nonlinear models such as the inviscid Burgers equation (Whitham, 1974) and has been followed in Gloerfelt *et al.* (2003) to compute the nonlinear propagation of the noise produced by the flow over a shallow cavity. It has been verified in preliminary tests that solving the weakly nonlinear Euler equations yields results very close to those obtained by solving the full Euler equations for wave amplitudes up to 10 000 Pa. Since the peak root mean square (rms) value of pressure levels on the extrapolation surface is 930 Pa, the present approximation is thus sufficient to reproduce the most important nonlinear propagation effects for the present jet. Finally, the effects of molecular absorption are not taken into account in the present model, as they would be significantly stronger than in experiments due to the small diameter of the simulated jet. As a result, the Gol'dberg number in the present simulation can be considered as infinite, which is not the case in the experiments. This simplification, however, facilitates the identification of nonlinear propagation effects in the acoustic field, as they are the only possible source of differences between the linear and nonlinear propagation models. The propagation equations are solved by using the same numerical methods as for the LES. At each time step, the fluctuation fields extracted from the LES are prescribed as boundary conditions at $r = 7.5D$, as well as at the inflow and outflow surfaces of the LES at $z = -0.75D$ and $z = 35D$, respectively. Near these boundaries, where centered finite difference schemes cannot be used, the spatial derivatives are computed using the non-centered schemes of Berland *et al.* (2007). In the nonlinear propagation, a shock-capturing procedure is applied at each time step to damp Gibbs oscillations near shocks. For that purpose, an adaptative filtering is applied. Its strength is computed based on the method presented in Sabatini *et al.* (2016). The computational domain for the extrapolations extends from $z = -10D$ down to $z = 100D$ in the axial direction and out to $100D$ in the radial direction. The axial and radial mesh spacings are equal to $\Delta r = \Delta z = 0.025D$, yielding a grid cutoff Strouhal number of 5, identical to that in the LES domain. In total, the grid contains $n_r \times n_\theta \times n_z = 4133 \times 64 \times 4480 = 1.19 \times 10^9$ points. After an initial transient period, the acoustic fields are recorded during a time of $1000D/u_j$ on eight planes of measurement points at $\theta = \theta_m$, with θ_m ranging from 0° to 315° by steps of 45°, and the statistical results are averaged in the azimuthal direction. The microphones are separated by a distance of $0.5D$ in the radial and axial directions, and the sampling frequency is equal to $fs = 17.4$ MHz, which corresponds to a Strouhal number of 5, identical to the grid cutoff frequency.

III. RESULTS

A. Snapshots and comparison with experiments

Snapshots of the pressure fluctuations from the LES and nonlinear extrapolation method are shown together in Fig. 1. Very directive wavefronts are generated and propagate at an angle of approximately 45° with respect to the flow direction. The region from which they originate spans a large extent of the plume, starting just downstream from the nozzle exit and ending at $z \simeq 30D$. These wavefronts are Mach waves generated by the supersonic convection of large-scale coherent structures in the jet (Tam, 1995; Troutt and Mclaughlin, 1982). They are expected to be the main cause of crackle as their generation process and nonlinear propagation promote the formation of shocks in the acoustic field.

The pressure spectra obtained for linear and nonlinear propagations at $r = 45D$ and $z = 65D$, in the region of the acoustic field where Mach wave radiation is dominant, are represented in Fig. 2. The measurements of Baars *et al.*

https://doi.org/10.1121/10.0003343

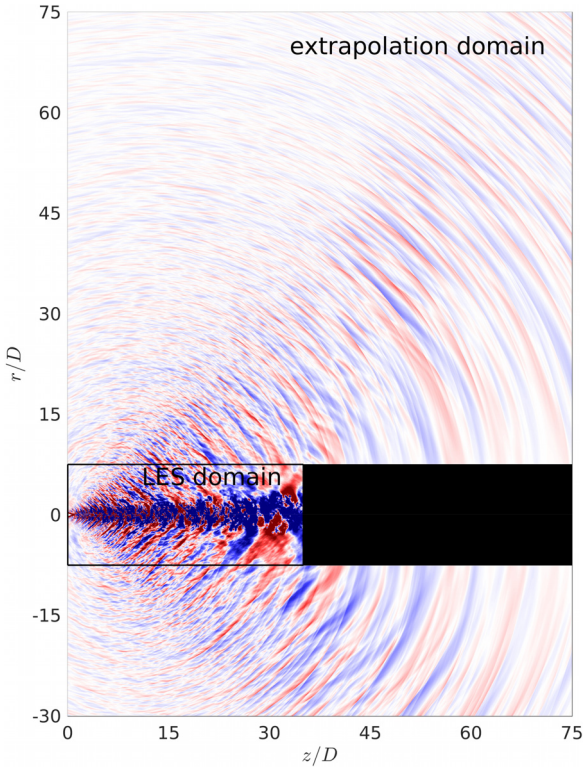

FIG. 1. (Color online) Snapshots of pressure fluctuations in the LES and extrapolation domains. The color scale ranges between ±3000 Pa.

(2014) for a cold Mach 3 jet are also indicated. The numerical and experimental spectra have very similar shapes. They all peak, in particular, at a Strouhal number of 0.15. The acoustic levels from the simulations are approximately 2 dB lower than those from the experiments. This can be explained by the fact that the boundary layers in the nozzle are weakly disturbed in the simulations but fully turbulent in the experiments. The pressure levels obtained for a nonlinear propagation are also lower than those for a linear propagation for Strouhal numbers between 0.15 and 1 but higher for Strouhal numbers higher than 1. This indicates that the Mach waves generated in the direction of peak levels are subject to nonlinear propagation effects, which are investigated in details in what follows.

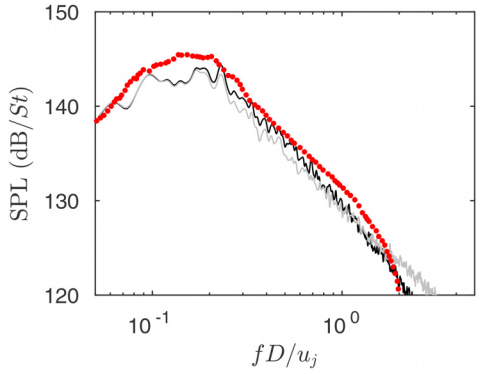

FIG. 2. (Color online) PSDs of the pressure fluctuations at $z = 65D$ and $r = 45D$ for linear (black line) and nonlinear (gray line) propagation. The red dots indicate the experimental measurements of Baars *et al.* (2014).

B. Spatial distribution of the acoustic levels

The rms values of the pressure fluctuations obtained for nonlinear propagation are represented in the (r, z) plane in Fig. 3. A peak due to Mach wave radiation is clearly visible in the downstream direction, as expected (Baars *et al.*, 2014; Troutt and Mclaughlin, 1982). To characterize the spatial structure of the acoustic field, a line and a circular array of microphones, displayed as red dashed lines in Fig. 3, are considered. As in the experimental studies of Baars *et al.* (2014) and Fiévet *et al.* (2016), the line array of microphones follows the path of peak noise levels. It originates at $z = 8.6D$ on the jet axis and has an angle of 48° with respect to the flow direction. The circular array is centered at the same point on the jet axis and has a radius of $80D$. It can be noted that the origin of the two arrays is significantly upstream from that in the experiments, located at $z = 17.5D$, suggesting that the distribution of the sound sources is not the same in the experiments and simulations. This is likely due to the different potential core lengths of the two jets, which are of $13D$ in the LES and of $20D$ in the experiments, because of the different initial states of the nozzle boundary layers.

The pressure levels on the circular array obtained in the numerical and experimental studies are plotted in Fig. 4. They are maximum for an angle close to 45° and are stronger for linear than for nonlinear propagation, as in de Cacqueray and Bogey (2014) and Langenais *et al.* (2019). As expected, the discrepancy between linear and nonlinear propagations is most important near the peak where the linearly predicted levels exceed the nonlinear ones by 2 dB. Despite the different origins of the circular and line arrays in the simulations and experiments, the results from the nonlinear simulations are in good agreement with the experimental data for polar angles lower than 60°, where crackle is expected to be strongest. This suggests that the sound sources in the simulated jets are located more upstream than in

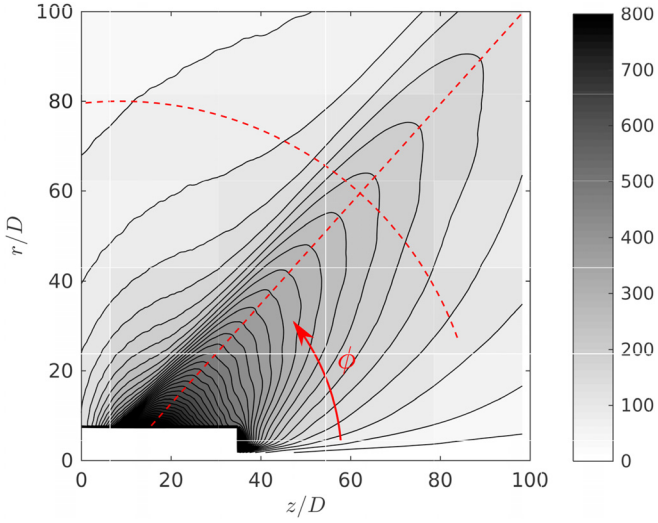

FIG. 3. (Color online) rms values of pressure fluctuations (in pascals) obtained for a nonlinear propagation. The linear and circular arrays are represented as red dashed lines.

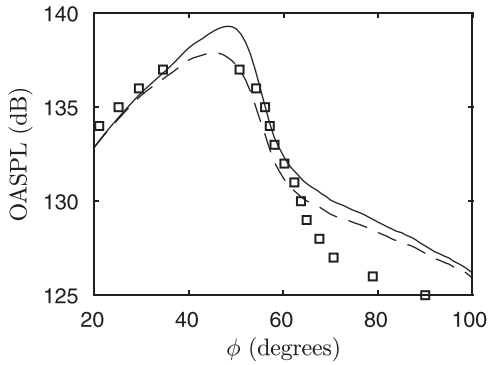

FIG. 4. Overall sound pressure levels on the circular array for linear (solid line) and nonlinear (dashed line) propagations. The squares indicate the experimental measurements of Baars *et al.* (2014).

the experiments but that the acoustic levels radiated along the path of peak noise levels are very similar. At higher angles, for $\phi \geq 60°$, the agreement between the simulations and experiments is poorer, which is likely due to the different states of the nozzle boundary layers, as previously observed for subsonic jets Bogey *et al.* (2012).

The pressure levels are represented as a function of the distance from the jet on the line array in Fig. 5. In the LES domain, on the left-hand side of the figure, the pressure levels decrease at a rate that is lower than the $1/r$-law derived for spherically spreading waves due to the fact that the sound sources are distributed over a wide extent of the jet flow. This decrease in the pressure levels is, however, slightly faster than the cylindrical decay predicted by Baars *et al.* (2016) and Fiévet *et al.* (2016) using a wavepacket model (Morris, 2009). In the propagation domain, on the right-hand side of the figure, the sound intensities predicted from the linear and nonlinear simulations are in good agreement in the vicinity of the LES domain, at $d \simeq 10D$. They diverge, however, for longer propagation distances so that the pressure levels for a linear propagation are approximately 2 dB louder than those for a nonlinear propagation at $d = 120D$. Far from the jet, for $z \geq 40D$, the pressure levels

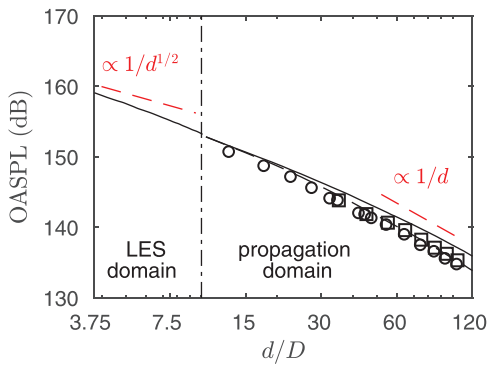

FIG. 5. (Color online) Overall sound pressure levels on the linear array (left from dashed-dotted line) for the LES and (right from dashed-dotted line) for the linear (solid line) and nonlinear (dashed line) propagations. The symbols indicate the experimental measurements of Baars *et al.* (2014) (squares) and Fiévet *et al.* (2016) (circles), and the dashed-dotted line indicates the limit between the LES and propagation domains.

decay at a rate close to the $1/r$-law derived for spherically spreading waves. It can also be noted that the location from which the pressure fluctuations decay according to a spherical law seems to be closer to the jet flow for the nonlinear propagation than for the linear one, which suggests that it is sensitive to the degree of nonlinearity in the waveforms. Finally, for the nonlinear propagation, the pressure levels on the path of peak noise are very close to those in the experiments, which confirms that the simulations reproduce well the acoustic waves radiated by the experimental jet along the line of peak pressure levels.

The PSDs of the acoustic pressure signals obtained on the linear array for propagation distances of $20D$, $40D$, $60D$, and $80D$ are plotted in Fig. 6 for the nonlinear propagation. They are scaled up to the levels obtained at $d = 80D$ assuming spherical spreading. The spectra are found to collapse very well for propagation distances longer than $40D$ and for Strouhal numbers higher than 0.2. This confirms that the pressure fluctuations along a linear array aligned with the path of peak noise levels can be considered as spherical for distances greater than $40D$, as observed by Fiévet *et al.* (2016). It can also be noted that the levels in the high-frequency range slightly increase with the propagation distance, as expected for a nonlinear propagation (de Cacqueray and Bogey, 2014).

C. Wave steepening and shock coalescence

1. Wave steepening

The nonlinear steepening of the acoustic waves radiated by the jet is investigated by comparing commonly used indicators of nonlinearity in the case of linear and nonlinear propagations. The signals recorded on the circular and line arrays are considered. The values of the skewness factor of the pressure fluctuations on the circular array are represented in Fig. 7(a). For all polar angles, they are positive and significantly deviate from the value of 0 expected for Gaussian signals, indicating a pronounced positive asymmetry of the fluctuations. This asymmetry is particularly strong near the peak of acoustic levels, at $\phi \simeq 45°$, where the skewness factor reaches the threshold value of 0.4 proposed by

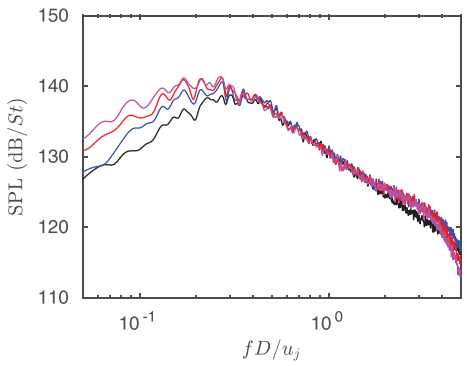

FIG. 6. (Color online) PSDs of the acoustic pressure for nonlinear propagation at $d = 20D$ (black line), $d = 40D$ (blue line), $d = 60D$ (red line), and $d = 80D$ (green line) on the linear array scaled at $d = 80D$, assuming spherical spreading.

https://doi.org/10.1121/10.0003343

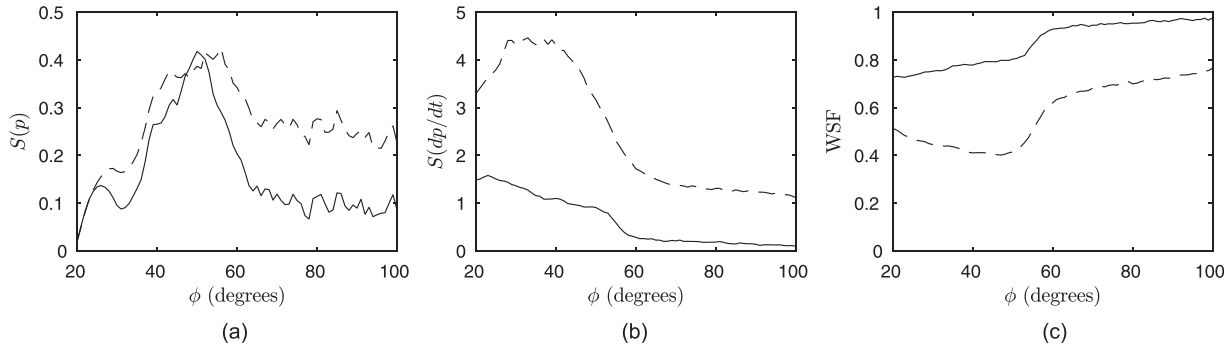

FIG. 7. Representation on the arc-array of the skewness factor of the pressure fluctuations (a), skewness factor of the pressure time derivative (b), and WSF (c) for linear (solid lines) and nonlinear (dashed lines) propagation.

Ffowcs Williams *et al.* (1975) for the onset of crackle. The peak value of the pressure skewness appears to be the same for linear and nonlinear propagations, indicating that the positive asymmetry of the waves radiated in this direction is mostly due to nonlinearities in the generation process of Mach waves, as described by Buchta and Freund (2019), and not to nonlinear propagation effects. For propagation angles higher than the peak angle, however, the skewness factor obtained for a nonlinear propagation is higher than the one obtained for a linear propagation, which suggests that nonlinear propagation effects increase the asymmetry of the pressure fluctuations for the waves propagating in the sideline direction.

The skewness factor of the pressure time derivative is represented in Fig. 7(b). Positive values are obtained for linear and nonlinear propagations, indicating the presence of steep compressions in the signals. The skewness factor of the pressure time derivative is significantly higher for a nonlinear than for a linear propagation, especially at polar angles lower than 60°. Indeed, as the propagation distance increases, nonlinear distortions promote the emergence of extreme, positive peaks of the pressure time derivative so that the skewness factor increases, as observed in Fiévet *et al.* (2016), Mora *et al.* (2014), and Gee *et al.* (2013). The WSF, defined as the ratio between the mean of the negative and positive values of the pressure time derivative (Gallagher and McLaughlin, 1981), is another measure of the steepened aspect of the waves. It is represented in Fig. 7(c) for the present signals. For linear and nonlinear propagations, the WSF is lower than the value 1 expected for smooth, harmonic waves, which indicates that the compressions in the pressure signals are steeper than the expansions. As expected, the WSF is significantly lower for a nonlinear than for a linear propagation as a result of nonlinear wave steepening. The decrease in the WSF can be seen for all polar angles and is most important around $\phi = 45°$, in the direction of peak noise levels.

The variations of the three indicators of nonlinearity on the line array are also represented in Fig. 8. In all cases, the values predicted for linear and nonlinear propagations are very close near the jet but diverge for longer propagation distances. In Fig. 8(a), the skewness factor of the pressure fluctuations peaks at $d \simeq 30D$ and then decreases with the propagation distance, as observed in Saxena *et al.* (2009). When the propagation is nonlinear, the peak skewness is slightly higher, and it decreases at a faster rate than when the propagation is linear. However, the difference between the skewness factors for linear and nonlinear propagation is small, thus confirming that the positive asymmetry of the pressure fluctuations is mainly a source effect. In Fig. 8(b), the skewness factor of the pressure time derivative decreases with the distance from the jet for a linear propagation but rapidly increases for a nonlinear propagation. In the nonlinear case, a rapid saturation is reached at $d \simeq 30D$, after which the skewness does not significantly vary with the propagation distance. Similarly, in Fig. 8(c), the WSF for a

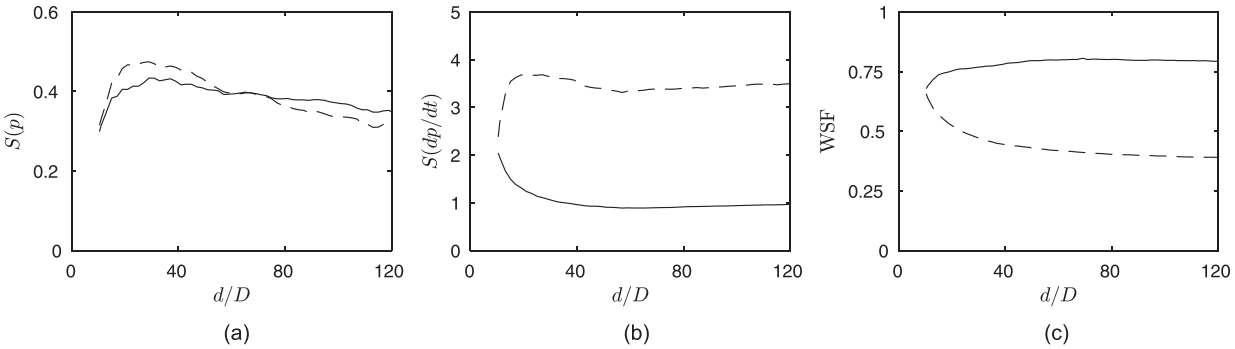

FIG. 8. Representation on the line array of the skewness factor of the pressure fluctuations (a), skewness factor of the pressure time derivative (b), and WSF (c) for linear (solid lines) and nonlinear (dashed lines) propagation.

nonlinear propagation decreases with the distance from the jet and reaches an asymptotic value of 0.4 for propagation distances greater than $80D$, which is much lower than the value of 0.75 obtained for a linear propagation. Therefore, while the acoustic waves radiated in the direction of peak levels present a steepened aspect near the source, they steepen even more with the propagation distance due to nonlinear propagation effects, in agreement with experiments (Fiévet *et al.*, 2016; Gallagher and McLaughlin, 1981; Petitjean *et al.*, 2006). Finally, for a linear propagation, it can be noted that the three nonlinearity indicators vary with the distance from the jet in the near acoustic field, for $d \leq 60D$, which can be surprising as there is no nonlinear wave steepening in this case. These variations are due to the fact that the pressure signals at a given measurement point include acoustic waves emitted from different regions of the jet flow. Since the tendency of the waves to present a steepened aspect near the source depends on the region from which they are generated (Pineau and Bogey, 2018), this will lead to variations of the nonlinearity indicators, even for a linear propagation.

2. Shock coalescence

The ZCR is defined as the mean number of zero-crossings in the pressure fluctuation signals recorded at a given position during a time of D/u_j. Its values on the line and circular arrays for linear and nonlinear propagations are plotted in Fig. 9. On the arc array, in Fig. 9(a), the ZCR is maximum at polar angles of 50° and 58° for linear and nonlinear propagations, respectively. In addition, the values obtained for a nonlinear propagation are lower than those for a linear propagation at all positions and, more particularly, close to the angle of peak noise levels, for a polar angle of 50°. On the line array, in Fig. 9(b), the ZCR for linear and nonlinear propagations are identical close to the jet flow, at $d = 10D$, but diverge for longer propagation distances, as the ZCR for a linear propagation increases while that for a nonlinear propagation decreases. The decrease in the ZCR for a nonlinear propagation can be explained by the coalescence of shocks in the jet acoustic field. Indeed, since the speed of sound increases with the local pressure, high amplitude peaks will aggregate those of smaller amplitudes as they propagate (Lighthill, 1994), thus causing a decrease in the ZCR, as observed in experimental measurements and numerical simulations of supersonic jets and free-shear flows (Buchta and Freund, 2017; Fiévet *et al.*, 2016; Gallagher and McLaughlin, 1981).

The difference between the ZCR obtained for linear and nonlinear propagations in the (r, z) plane is shown in Fig. 10 to directly determine the regions of the jet acoustic field where shock coalescence is strongest. This difference is negative at all of the positions considered, which indicates that shock coalescence occurs everywhere in the jet acoustic field. It is, however, particularly, important along a narrow cone located slightly upstream from the line of peak acoustic levels.

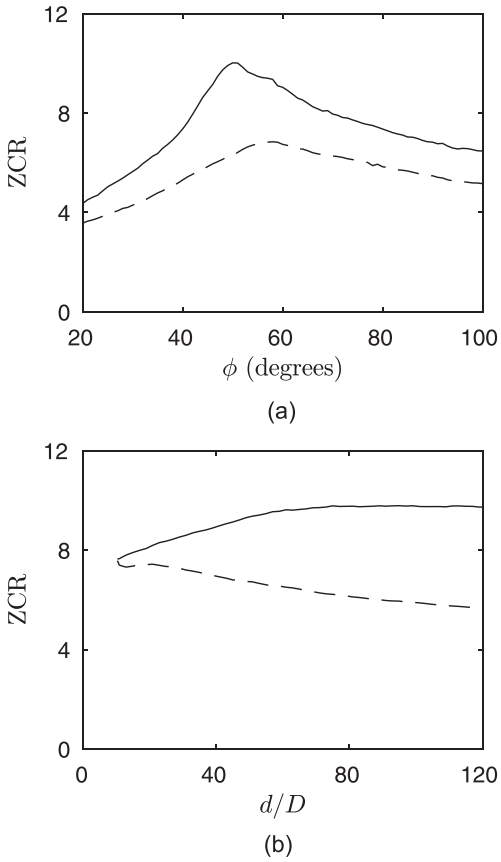

FIG. 9. Mean number of zero-crossings during a time $t = D/u_j$ on the circular (a) and line (b) arrays for linear (solid lines) and nonlinear (dashed lines) propagations.

D. Effects of nonlinear propagation on pressure signals and spectra

The effects of wave steepening and shock coalescence on the pressure signals and spectra are now investigated. For that, the signals recorded on the line array at distances

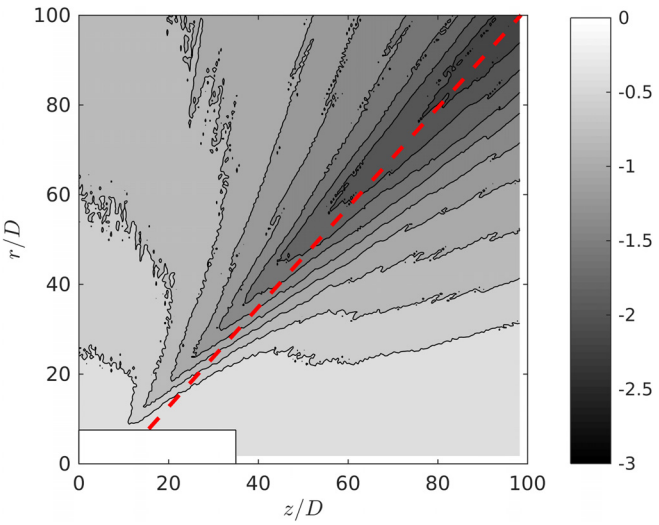

FIG. 10. (Color online) Difference between the mean number of zero-crossings during a time $t = D/u_j$ obtained for nonlinear and linear propagations. The line of peak pressure levels is represented as a red dashed line.

https://doi.org/10.1121/10.0003343

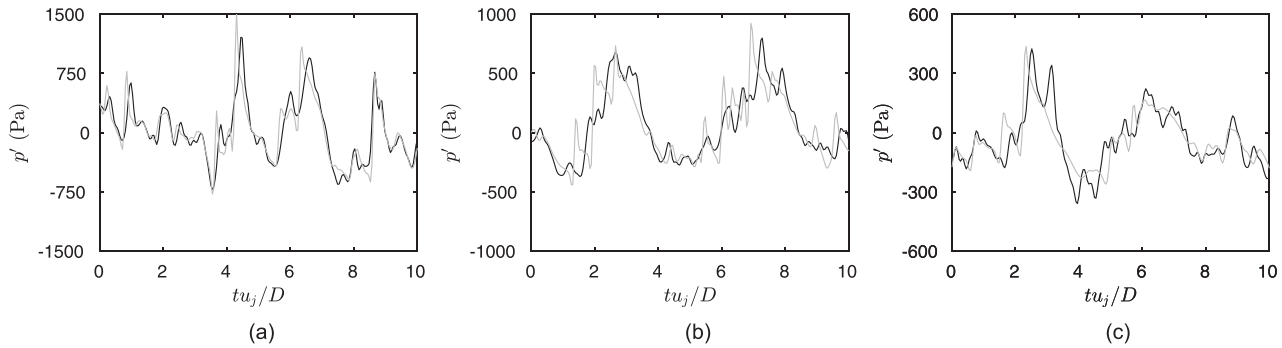

FIG. 11. Pressure fluctuations at $d = 20D$ (a), $40D$ (b), and $80D$ (c) on the linear array for linear (black line) and nonlinear (gray line) propagation.

$d = 20D$, $40D$, and $80D$ are plotted in Fig. 11 for linear and nonlinear propagations. In the two cases, distinctive, positively skewed shock-like structures are present in the signals as, for instance, at $t = 2D/u_j$ and $6D/u_j$ in Fig. 11(b). The pressure signals for linear and nonlinear propagations are very similar at $d = 20D$ but differ for larger distances, for $d = 40D$ and $80D$. At these locations, the pressure peaks for a nonlinear propagation are found earlier in the signals than those for a linear propagation, since the speed of sound increases with the local pressure, according to Eq. (2). In addition, compressions in the signals are also much steeper as a result of nonlinear propagation effects, which is consistent with the rise of the skewness factor of the pressure time derivative as well as with the decrease in the WSF. Finally, at $d = 80D$ in Fig. 11(c), the signal for a linear propagation displays two pressure peaks between $t = 2D/u_j$ and $4D/u_j$, whereas only one peak is visible in the signal obtained for a nonlinear propagation. This is likely due to the merging of the two peaks, i.e., to shock coalescence.

PSDs of the pressure fluctuations signals on the line array are shown in Fig. 12, at the same positions as those in Fig. 11. Near the jets, at $d = 20D$ in Fig. 12(a), the pressure spectra obtained for linear and nonlinear propagations are similar in the low- and medium-frequency ranges, up to a Strouhal number of 1, but differ in the high-frequency range where the levels for a nonlinear propagation are higher than those for linear propagation. This is also the case at $d = 40D$ in Fig. 12(b) and $d = 80D$ in Fig. 12(c). At these locations, the spectra for a nonlinear propagation also exhibit lower levels than those for a linear propagation in the medium-frequency range, for Strouhal numbers between 0.3 and 1, suggesting a power transfer from the middle to the high frequencies, which is consistent with nonlinear wave steepening. Moreover, for the largest propagation distance, in Fig. 12(c), the peak Strouhal number is slightly lower for a nonlinear propagation than for a linear propagation, which can be explained by the coalescence of shocks in the signals. Finally, in Fig. 12(c), the PSD for nonlinear propagation decays at a rate very close to the power law St^{-2} in the medium-frequency range. This observation is in agreement with analytical predictions (Gurbatov and Rudenko, 1998) and experimental measurements (McInerny and Ölçmen, 2005) of the nonlinear evolution of broadband acoustic waveforms.

To measure the cumulated importance of nonlinear propagation effects in the signals recorded at a given point, the power deficit rate (PDR) is defined as the difference of power between the signals obtained for a nonlinear and a linear propagation, integrated over frequencies for which the noise levels are lower for a nonlinear than for a linear propagation. It is normalized by the sound intensity for a linear propagation and can thus be interpreted as the fraction of power in the linear signal transferred to the high or low frequencies in the nonlinear case because of wave steepening and shock coalescence. It is computed using the following relation,

$$\mathrm{PDR} = \left| t \frac{\int_0^\infty \min\left\{ S_{pp}^{nlin}(f) - S_{pp}^{lin}(f), 0 \right\} \mathrm{d}f}{\int_0^\infty S_{pp}^{lin}(f) \mathrm{d}f} \right| t, \tag{3}$$

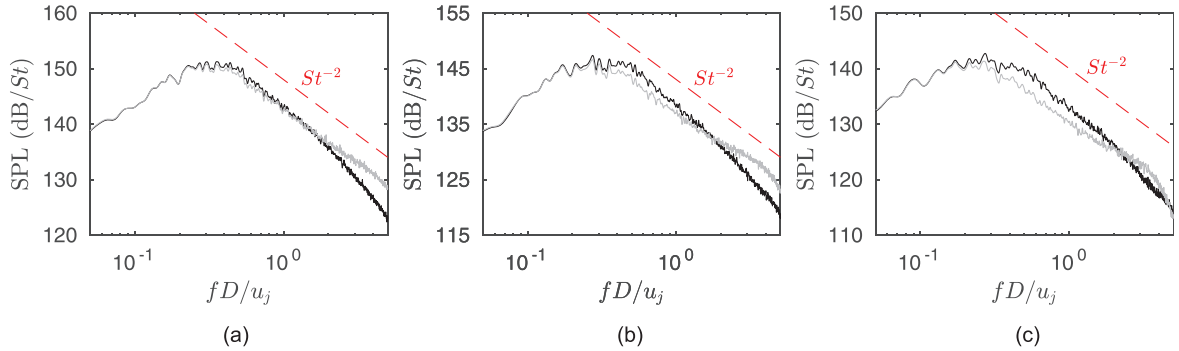

FIG. 12. (Color online) PSDs of pressure fluctuations on the linear array at $d = 20D$ (a), $40D$ (b), and $80D$ (c) for a linear (black line) and nonlinear (gray line) propagation.

where S_{pp}^{lin} and S_{pp}^{nlin} are the PSDs of the pressure fluctuations for linear and nonlinear propagations, respectively. The values of the PDR in the (r, z) plane are plotted in Fig. 13. They are close to 0 near the LES domain, for short propagation distances, but increase with the distance from the jet. Significant values are obtained at all propagation angles. They are, however, particularly high near a narrow cone located slightly upstream of the path of peak noise levels, which is also where shock coalescence is the most frequent in Fig. 10. Along this cone, the rise of the PDR is rapid close to the jet but is more gradual as the propagation distance increases due to decrease in the pressure levels.

It is noteworthy that the region of the jet acoustic field where the nonlinear power transfer is strongest is not aligned with the line of peak levels. To investigate this, the shock formation distance is estimated for different axial positions at $r = 7.5D$ as an indicator of the tendency of the waves to propagate nonlinearly. The expression proposed by Gurbatov and Rudenko (1998) for plane, broadband waves is used:

$$\bar{x} = \frac{\rho_\infty a_\infty^3}{\beta(2\pi f_{max}) p_{rms}}, \tag{4}$$

where $f_{\max}$ is the peak frequency of the signal and $\beta = (\gamma + 1)/2$. It can be noted that this expression is not strictly valid for diverging waves. Expressions of the shock formation distance have been derived for the case of spherical or cylindrical diverging waves, as in Hamilton (2016). However, they involve the location of the source, which is not known in the present case. Thus, since the objective here is to compare the tendency of the waves to propagate nonlinearly and not to estimate actual shock formation distances, the expression (4) for plane waves is used for the sake of simplicity. This is justified, since the shock formation distance for diverging waves is an increasing function of the right-hand side of Eq. (4). Based on this expression, the shock formation distance decreases with the amplitude of the pressure fluctuations, as well as with their peak frequency.

The peak Strouhal number of the pressure fluctuations $f_{\max}D/u_j$ at the outward limit of the LES domain is represented in Fig. 14(a) as a function of the axial distance. It reaches a clear peak of 0.8 at $z = 10D$ which is much higher than the value of 0.4 obtained near the maximum of pressure levels at $z = 14D$. This peak is due to the generation of high-frequency waves by the shear layers of the jet (Baars *et al.*, 2014). The axial variations of the shock formation distance at the same locations are plotted in Fig. 14(b). It reaches a minimum of $\bar{x} = 20D$ near $z \simeq 10D$, which is slightly upstream from the location of peak noise levels but close to that where the signal peak frequency is highest. It is also very close to the origin of the cone of PDR in Fig. 13. Upstream and downstream from this minimum, the shock formation distance, can, however, be higher than $100D$ so that nonlinear propagation effects are weak. Therefore, waves generated near the nozzle, which have high frequencies and amplitudes, steepen more rapidly than those produced near the peak, which have higher levels but lower frequencies. This explains why the most strongly nonlinear waves are located slightly upstream from the line of peak levels.

E. Morfey–Howell indicator

The power transfers due to nonlinear propagation are evaluated by considering the Morfey–Howell indicator

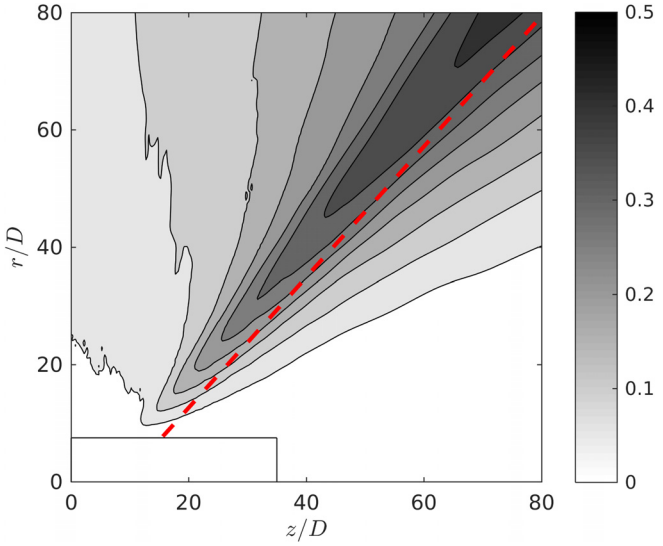

FIG. 13. (Color online) Power deficit rate in the (r, z) plane. The line of peak pressure levels is represented as a red dashed line.

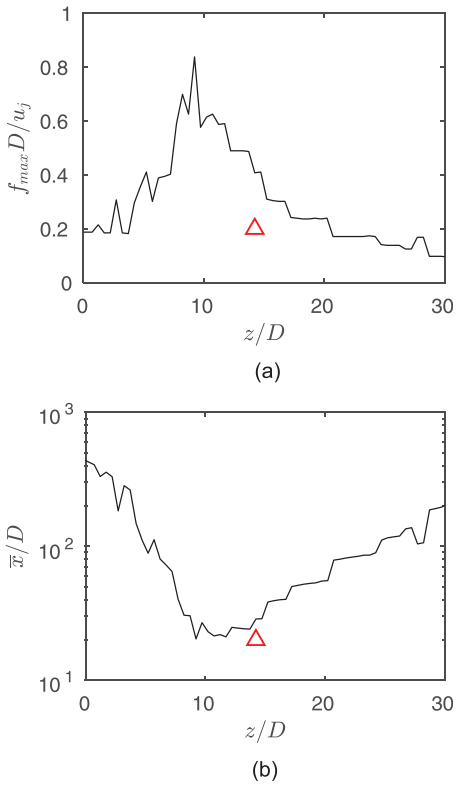

FIG. 14. (Color online) Axial variations at $r = 7.5D$ of the peak Strouhal number of the pressure fluctuations (a) and shock formation distance (b). The red triangles indicate the location of peak acoustic levels.

https://doi.org/10.1121/10.0003343

(Baars *et al.*, 2014; Morfey and Howell, 1981; Petitjean *et al.*, 2006). This indicator is defined as $Q_{p^2p}(f) = -\mathrm{Im}\{2\hat{p}_2(f)\hat{p}^\star(f)\}$, where $\hat{p}(f)$ and $\hat{p}_2(f)$ are the Fourier transforms of $p(t)$ and $p^2(t)$, respectively. By using a generalized Burgers equation for spherically spreading waves, Morfey and Howell (1981) related this quantity to the derivative of the signal PSD with respect to the radial direction:

$$\frac{\partial}{\partial r}\left(r^2 e^{2\alpha r} S_{pp}\right) = \left(2\pi f \frac{\beta}{\rho_\infty a_\infty^3}\right) r^2 e^{2\alpha r} Q_{p^2p}, \tag{5}$$

where $\beta = (\gamma+1)/2$ and α is the linear attenuation. According to Eq. (5), this indicator measures the flux of power transfers due to nonlinear distortions: negative values for a given frequency indicate a loss of power for that frequency, whereas positive ones reveal a gain of power. In practice, predictions of nonlinear propagation effects based on the Morfey–Howell indicator at a single point can be difficult to interpret. Indeed, separating the effects of nonlinearities, geometrical spreading, and molecular absorption based on Eq. (5) only is not straightforward. For this reason, Reichman *et al.* (2016) rearranged Eq. (5) so that the spatial rate of change of the pressure levels is the sum of three contributions associated with nonlinearities, geometrical spreading, and molecular absorption and derived a single-point nonlinearity indicator accounting for the effects of nonlinearities only (Gee *et al.*, 2018b; Miller and Gee, 2018). Another issue is that while Q_{p^2p} measures the degree of quadratic nonlinear interactions in the waveforms, nonlinear propagation effects are not the only mechanism that can cause such interactions. Notably, the pressure signals near supersonic jets are known to display shock-like structures that are formed inside the jet flow due to a source steepening mechanism (Buchta and Freund, 2017; Nichols *et al.*, 2013; Pineau and Bogey, 2019). This will lead to non-zero values of the Morfey–Howell indicator for a linear propagation. Thus, it has been pointed out that the indicator must be estimated at several positions to assess the presence of nonlinear propagation effects (Baars *et al.*, 2014; Howell and Morfey, 1987). Finally, the physical interpretation relies on the assumption that the waves are spherical. This is not the case in the near field of supersonic jets, where the pressure fluctuations include acoustic waves emitted from different regions of the jet flow, propagating along different rays. For these reasons, in the present work, the spatial distribution of the Morfey–Howell indicator is considered in the (r, z) plane and not only along a given propagation path as in most studies. The values obtained for linear and nonlinear propagations are also compared so that any difference between the Morfey–Howell indicators computed for nonlinear and linear propagations can be directly attributed to nonlinear distortions.

The Morfey–Howell indicator obtained for a linear propagation is represented in Fig. 15 for Strouhal numbers of 0.5, 1, and 2. Since the values of Q_{p^2p} depend on the sound intensity, the normalized version Q/S of the indicator is considered, with $Q = Q_{p^2p}/p_{\mathrm{rms}}^3$ and $S = S_{pp}/p_{\mathrm{rms}}^2$. This quantity is useful, as it can be directly related to the dissipation of power arising because of nonlinearities (Morfey and Howell, 1981; Ohm *et al.*, 2020). For a Strouhal number of 0.5, in Fig. 15(a), Q/S displays negative values near the peak of acoustic levels, while the values away from the maximum are much lower in absolute value. For a Strouhal number of 1 in Fig. 15(b), the indicator Q/S has strong negative values over a very narrow band slightly upstream from the peak of acoustic levels but positive ones at low polar angles. Finally, for a Strouhal number of 2, Q/S is positive for polar angles below and near the line of peak acoustic levels. The fact that the Morfey–Howell indicator exhibits significant values for a linear propagation indicates that the input waveforms present a certain degree of nonlinearity near the LES interface that remains unchanged during the linear propagation. This is also reflected in the values of the skewness factors of the pressure fluctuations and of their time derivative in Figs. 7 and 8, which are significant, even for a linear propagation. This is either due to nonlinear distortions occurring over short distances inside the LES domain or due to the generation of shocks directly from the jet flow, as described in Buchta and Freund (2017) and Pineau and Bogey (2019).

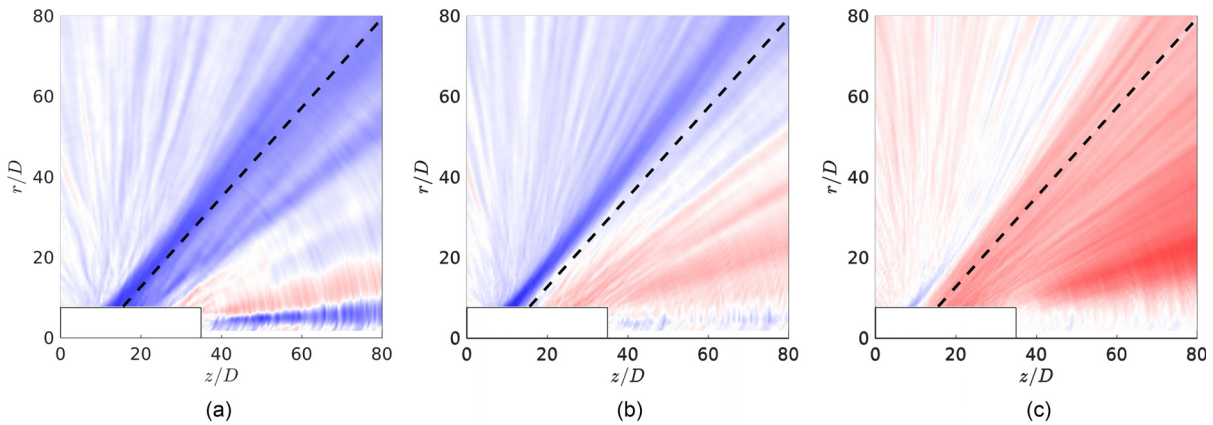

FIG. 15. (Color online) Representation of the Morfey–Howell nonlinearity indicator Q/S for a linear propagation for Strouhal numbers of 0.5 (a), 1 (b), and 2 (c). The color scale ranges between ± 1, from blue to red. The line of peak pressure levels is represented as a red dashed line.

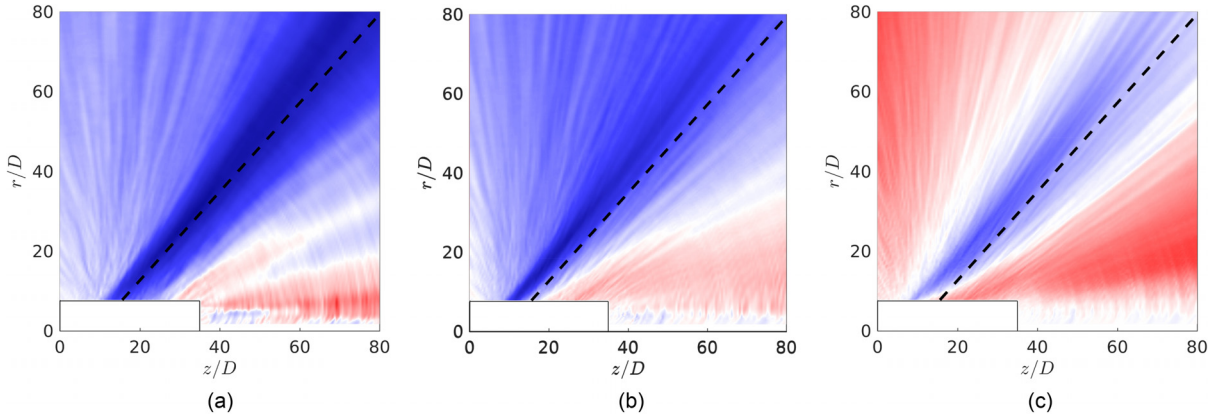

FIG. 16. (Color online) Representation of the Morfey–Howell nonlinearity indicator Q/S for a nonlinear propagation for Strouhal numbers of 0.5 (a), 1 (b), and 2 (c). The color scale ranges between ± 1, from blue to red. The line of peak pressure levels is represented as a red dashed line.

The Morfey–Howell indicator calculated from the pressure fields obtained for a nonlinear propagation is represented in Fig. 16 for the same three Strouhal numbers as previously. For a Strouhal number of 0.5, in Fig. 16(a), strong negative values of Q/S are obtained near the peak of acoustic levels. This is also the case for a Strouhal number of 1, in Fig. 16(b). These negative values are much stronger than for a linear propagation. This indicates a nonlinear power loss from the middle frequencies as the waves propagate. For a Strouhal number of 1, in Fig. 16(b), positive values are also obtained at low polar angles. At these angles, the peak frequencies are indeed lower than those near the peak of rms. Thus, nonlinear distortions tend to transfer power from the low frequencies to the $St = 1$ component. The values of the Morfey–Howell indicator are, however, only very slightly higher than those for a linear propagation, suggesting that nonlinear distortions are weak for waves propagating in that direction. Finally, for a Strouhal number of 2, in Fig. 16(c), Q/S is negative close to the line of peak pressure levels but positive away from the peak. This is in stark contrast with the distribution for a linear propagation in Fig. 15(c), where Q/S is positive all over the acoustic field. This demonstrates that power is lost for a Strouhal number of 2 in the direction of peak noise level because of nonlinear propagation effects. This power is then transmitted to higher frequencies, leading to the formation of shocks. At high polar angles, the positive values of Q/S are much stronger than for a linear propagation, which is also indicative of nonlinear propagation effects. For these angles, the Morfey–Howell indicator is positive, which means that the $St = 2$ component receives power from the lower frequencies.

Finally, the nonlinear power transfers can be measured directly by considering the difference between the PSD obtained for nonlinear and linear propagations. Unlike the Morfey–Howell indicator, which predicts the flux of power transfer based on the degree of quadratic nonlinear interaction in the waveforms, this approach provides a direct way to assess the effects of nonlinear distortions on the pressure spectra. It can thus be used as a reference. In Fig. 17, the spatial distribution of the difference between the PSD for nonlinear and linear propagations is represented for a Strouhal number of 1. It is normalized by the PSD obtained for a linear propagation to take into account the decrease in the pressure levels with the propagation distance. Negative values are obtained at high polar angles and are strongest, in absolute value, near the peak of acoustic levels. Low-amplitude, positive values are, however, obtained at lower polar angles. Negative values at a given point indicate that power is lost during the nonlinear propagation of the waves, whereas positive ones reveal a gain of power. Therefore, the power transfers directly evaluated by comparing the spectra for nonlinear and linear propagations are, qualitatively, in very good agreement with the flux estimated using the Morfey–Howell indicator for the same Strouhal number in Fig. 16(b). This suggests that considering the spatial distribution of the Morfey–Howell indicator for individual frequencies can provide reliable estimations of the direction of nonlinear power flux in the sound field of supersonic jets, even in the jet near field, where the spherical-wave hypothesis is not strictly verified.

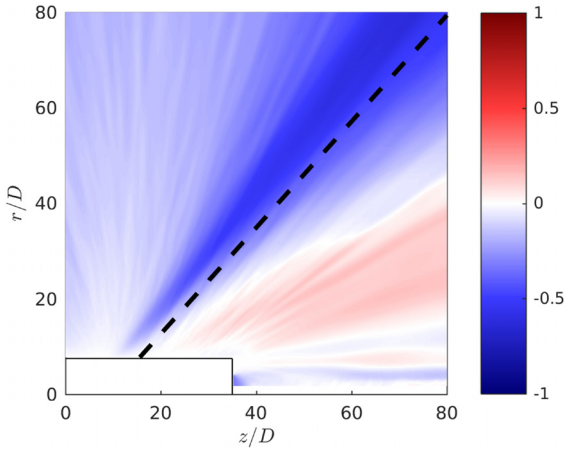

FIG. 17. (Color online) Difference between the PSD for a nonlinear and a linear propagation for a Strouhal number of 1 normalized by the PSD for a linear propagation. The red dashed line indicates the line of peak acoustic levels.

https://doi.org/10.1121/10.0003343

IV. CONCLUSION

In the present study, the effects of nonlinear propagation on the acoustic waves emitted by a cold Mach 3 jet are investigated using numerical simulations. The jet flow and near acoustic fields are computed using LES, while the acoustic field is propagated to the far field by solving the loss-less linearized and weakly nonlinear Euler equations, respectively. By comparing the pressure signals obtained for linear and nonlinear propagations, this approach allows us to directly identify the effects of nonlinear distortions on the acoustic waves generated by the jet. Near the peak of pressure levels, these waves present a strong positive asymmetry that does not seem to depend on the linear or the nonlinear propagations of the waves. This confirms that this asymmetry is the consequence of a source mechanism occurring inside the turbulent jet flow, as suggested by previous investigations (Buchta and Freund, 2017; Ffowcs Williams *et al*., 1975; Fiévet *et al*., 2016), and not that of nonlinear propagation effects. A different conclusion is, however, reached for the steepened aspect of the waves, which is evaluated by computing the skewness factor of the pressure time derivative and the WSF. Indeed, while the signals for a linear propagation present a steepened aspect due to the source steepening mechanism, this aspect is much more pronounced for a nonlinear propagation than for a linear one because of the formation of shocks. For a nonlinear propagation, the number of zero-crossings also decreases with the propagation distance, which is attributed to the coalescence of shocks, as observed in previous experiments (Fiévet *et al*., 2016; Gallagher and McLaughlin, 1981). The present results thus highlight the importance of nonlinear wave steepening in the formation process of the steepened waves at the origin of crackle noise. In particular, the fact that the skewness factor of the pressure time derivative, which has been found to correlate well with the perception of crackle (Gee *et al*., 2018a), is much higher for the nonlinear propagation than for the linear one advocates that nonlinearities play a key role in the perception of crackle. However, since the present simulations do not include the effects of molecular absorption, additional studies at finite Gol'dberg numbers are required to confirm that it is the dominant mechanism.

Finally, the nonlinear transfer of power from the middle- to the high- and low-frequency components of the spectra due to wave steepening and shock coalescence, respectively, are investigated. These transfers are first predicted by considering the distribution of the Morfey–Howell nonlinearity indicator in the (r, z) plane for linear and nonlinear propagations. Then nonlinear power transfers are directly measured by comparing the spectra for a nonlinear and a linear propagation. These measurements are found to be in good qualitative agreement with the predictions based on the Morfey–Howell indicators. More surprisingly, this is also the case in the jet near field, where the spherical-wave hypothesis is not verified. This advocates for the use of the Morfey–Howell indicator to predict nonlinear distortions in the near acoustic field of supersonic jets, even when its underlying assumptions are not strictly verified.

ACKNOWLEDGMENTS

This work was granted access to the HPC resources of PMCS2I (Pôle de Modélisation et de Calcul en Sciences de l'Ingénieur et de l'Information) of Ecole Centrale de Lyon, PSMN (Pôle Scientifique de Modélisation Numérique) of ENS de Lyon and P2CHPD (Pôle de Calcul Hautes Performances Dédiés) of Université Lyon I, members of FLMSN (Fédération Lyonnaise de Modélisation et Sciences Numériques), partner of EQUIPEX EQUIP@MESO, and to the resources of IDRIS (Institut du Développement et des Ressources en Informatique Scientifique) under the allocation 2019-2a0204 made by GENCI (Grand Equipement National de Calcul Intensif). It was performed within the framework of the Labex CeLyA of Université de Lyon, within the programme "Investissements d'Avenir" (ANR-10-LABX-0060/ANR-16-IDEX-0005) operated by the French National Research Agency (ANR).

Baars, W., Tinney, C., Wochner, M., and Hamilton, M. (**2014**). "On cumulative nonlinear acoustic waveform distortions from high-speed jets," J. Fluid Mech. **749**, 331–366.
Baars, W. J., and Tinney, C. E. (**2014**). "Shock-structures in the acoustic field of a Mach 3 jet with crackle," J. Sound Vib. **333**(12), 2539–2553.
Baars, W. J., Tinney, C. E., and Hamilton, M. F. (**2016**). "Piecewise-spreading regime model for calculating effective Gol'dberg numbers for supersonic jet noise," AIAA J. **54**(9), 2833–2842.
Berland, J., Bogey, C., Marsden, O., and Bailly, C. (**2007**). "High-order, low dispersive and low dissipative explicit schemes for multiple-scale and boundary problems," J. Comput. Phys. **224**(2), 637–662.
Bogey, C., and Bailly, C. (**2002**). "Three-dimensional non-reflective boundary conditions for acoustic simulations: Far field formulation and validation test cases," Acta Acust. **88**(4), 463–471.
Bogey, C., and Bailly, C. (**2004**). "A family of low dispersive and low dissipative explicit schemes for flow and noise computations," J. Comput. Phys. **194**(1), 194–214.
Bogey, C., and Bailly, C. (**2006**). "Computation of a high Reynolds number jet and its radiated noise using large eddy simulation based on explicit filtering," Comput. Fluids **35**(10), 1344–1358.
Bogey, C., and Bailly, C. (**2009**). "Turbulence and energy budget in a self-preserving round jet: Direct evaluation using large eddy simulation," J. Fluid Mech. **627**, 129–160.
Bogey, C., de Cacqueray, N., and Bailly, C. (**2009**). "A shock-capturing methodology based on adaptative spatial filtering for high-order non-linear computations," J. Comput. Phys. **228**(5), 1447–1465.
Bogey, C., de Cacqueray, N., and Bailly, C. (**2011a**). "Finite differences for coarse azimuthal discretization and for reduction of effective resolution near origin of cylindrical flow equations," J. Comput. Phys. **230**(4), 1134–1146.
Bogey, C., Marsden, O., and Bailly, C. (**2011b**). "Large-eddy simulation of the flow and acoustic fields of a Reynolds number 10^5 subsonic jet with tripped exit boundary layers," Phys. Fluids **23**(3), 035104.
Bogey, C., Marsden, O., and Bailly, C. (**2012**). "Influence of initial turbulence level on the flow and sound fields of a subsonic jet at a diameter-based Reynolds number of 10^5," J. Fluid Mech. **701**, 352–385.
Buchta, D. A., and Freund, J. B. (**2017**). "The near-field pressure radiated by planar high-speed free-shear-flow turbulence," J. Fluid Mech. **832**, 383–408.
Buchta, D. A., and Freund, J. B. (**2019**). "Intense sound radiation by high-speed flow: Turbulence structure, gas properties, and near-field gas dynamics," Phys. Rev. Fluids **4**, 044605.
Crighton, D., and Bashforth, S. (**1980**). "Nonlinear propagation of broadband jet noise," *Proceedings of the 6th Aeroacoustics Conference*, June 4–6, Hartford, CT, AIAA paper 1980-1039.

de Cacqueray, N., and Bogey, C. (**2014**). "Noise of an overexpanded Mach 3.3 jet: Non-linear propagation effects and correlations with flow," Int. J. Aeroacoust. **13**(7-8), 607–632.
Ffowcs Williams, J. E., Simson, J., and Virchis, V. J. (**1975**). "'Crackle': An annoying component of jet noise," J. Fluid Mech. **71**(2), 251–271.
Fiévet, R., Tinney, C. E., Baars, W. J., and Hamilton, M. F. (**2016**). "Coalescence in the sound field of a laboratory-scale supersonic jet," AIAA J. **54**(1), 254–265.
Gallagher, J., and McLaughlin, D. (**1981**). "Experiments on the nonlinear characteristics of noise propagation from low and moderate Reynolds number supersonic jets," *Proceedings of the 7th Aeroacoustics Conference*, October 5–7, Palo Alto, CA, AIAA Paper 1981-2041.
Gee, K. L., Miller, K. G., Reichman, B. O., and Wall, A. T. (**2018a**). "Frequency-domain nonlinearity analysis of noise from a high-performance jet aircraft," Proc. Meet. Acoust. **34**(1), 045027.
Gee, K. L., Neilsen, T. B., Downing, J. M., James, M. M., McKinley, R. L., McKinley, R. C., and Wall, A. T. (**2013**). "Near-field shock formation in noise propagation from a high-power jet aircraft," J. Acoust. Soc. Am. **133**(2), EL88–EL93.
Gee, K. L., Russavage, P. B., Neilsen, T. B., Hales Swift, S., and Vaughn, A. B. (**2018b**). "Subjective rating of the jet noise crackle percept," J. Acoust. Soc. Am. **144**(1), EL40–EL45.
Gee, K. L., Sparrow, V. W., James, M. M., Downing, J. M., Hobbs, C. M., Gabrielson, T. B., and Atchley, A. A. (**2008**). "The role of nonlinear effects in the propagation of noise from high-power jet aircraft," J. Acoust. Soc. Am. **123**(6), 4082–4093.
Gloerfelt, X., Bogey, C., and Bailly, C. (**2003**). "Numerical evidence of mode switching in the flow-induced oscillations by a cavity," Int. J. Aeroacoust. **2**(2), 193–217.
Hamilton, M. F. (**2016**). "Effective Gol'dberg numbers for diverging waves," J. Acoust. Soc. Am. **140**(6), 4419–4426.
Howell, G. P., and Morfey, C. L. (**1987**). "Non-linear propagation of broadband noise signals," J. Sound Vib. **114**(2), 189–201.
Gurbatov, S. N., and Rudenko, O. V. (**1998**). "Statistical phenomena," in *Nonlinear Acoustics*, edited by M. F. Hamilton and D. T. Blackstock (Academic, San Diego, CA), Chap. 13, pp. 377–398.
Krothapalli, A., Greska, B., and Arakeri, V. (**2002**). "High speed jet noise reduction using microjets," *Proceedings of the 8th AIAA/CEAS Aeroacoustics Conference and Exhibit*, June 17–19, Breckenridge, CO, AIAA Paper 2002-2450.
Krothapalli, A., Venkatakrishnan, L., and Lourenco, L. (**2000**). "Crackle: A dominant component of supersonic jet mixing noise," Proceedings of the 6*th Aeroacoustics Conference and Exhibit*, June 12–14, Lahaina, HI, AIAA Paper 2000-2024.
Kuo, C.-W., Veltin, J., and McLaughlin, D. K. (**2012**). "Effects of jet noise source distribution on acoustic far-field measurements," Int. J. Aeroacoust. **11**(7-8), 885–915.
Langenais, A., Vuillot, F., Troyes, J., and Bailly, C. (**2019**). "Accurate simulation of the noise generated by a hot supersonic jet including turbulence tripping and nonlinear acoustic propagation," Phys. Fluids **31**(1), 016105.
Lighthill, J. (**1994**). "The inaugural Theodorsen lecture," Theoret. Comput. Fluid Dyn. **6**, 261–280.
Lowson, M. V., and Ollerhead, J. B. (**1968**). "Visualization of noise from cold supersonic jets," J. Acoust. Soc. Am. **44**(2), 624–630.
Martens, S., Spyropoulos, J. T., and Nagel, Z. (**2011**). "The effect of chevrons on crackle: Engine and scale model results," *Proceedings of the ASME 2011 Turbo Expo: Turbine Technical Conference and Exposition. Volume 1: Aircraft Engine; Ceramics; Coal, Biomass and Alternative Fuels; Wind Turbine Technology*, June 6–10, Vancouver, BC, Canada, pp. 315–326.
McInerny, S. A. (**1996**). "Launch vehicle acoustics. II - statistics of the time domain data," J. Aircraft **33**(3), 518–523.
McInerny, S. A., and Ölçmen, S. M. (**2005**). "High-intensity rocket noise: Nonlinear propagation, atmospheric absorption, and characterization," J. Acoust. Soc. Am. **117**(2), 578–591.
Miller, K. G., and Gee, K. L. (**2018**). "Model-scale jet noise analysis with a single-point, frequency-domain nonlinearity indicator," J. Acoust. Soc. Am. **143**(6), 3479–3492.
Mohseni, K., and Colonius, T. (**2000**). "Numerical treatment of polar coordinate singularities," J. Comput. Phys. **157**(2), 787–795.
Mora, P., Heeb, N., Kastner, J., Gutmark, E. J., and Kailasanath, K. (**2014**). "Impact of heat on the pressure skewness and kurtosis in supersonic jets," AIAA J. **52**(4), 777–787.
Morfey, C. L., and Howell, G. P. (**1981**). "Nonlinear propagation of aircraft noise in the atmosphere," AIAA J. **19**(8), 986–992.
Morris, P. J. (**2009**). "A note on noise generation by large scale turbulent structures in subsonic and supersonic jets," Int. J. Aeroacoust. **8**(4), 301–315.
Murray, N. E., and Lyons, G. W. (**2016**). "On the convection velocity of source events related to supersonic jet crackle," J. Fluid Mech. **793**, 477–503.
Nichols, J. W., Lele, S. K., Ham, F. E., Martens, S., and Spyropoulos, J. T. (**2013**). "Crackle noise in heated supersonic jets," J. Eng. Gas Turb. Pow. **135**(5), 051202.
Ohm, W.-S., Gee, K. L., and Park, T. (**2020**). "An impedance-based formulation of frequency-domain nonlinearity indicators in finite amplitude sound propagation," J. Acoust. Soc. Am. **148**(3), EL295–EL300.
Papamoschou, D. (**1995**). "Evidence of shocklets in a counterflow supersonic shear layer," Phys. Fluids **7**(2), 233–235.
Petitjean, B. P., Viswanathan, K., and McLaughlin, D. K. (**2006**). "Acoustic pressure waveforms measured in high speed jet noise experiencing nonlinear propagation," Int. J. Aeroacoust. **5**(2), 193–215.
Pineau, P., and Bogey, C. (**2018**). "Study of the generation of shocks by high-speed jets using conditional averaging," *Proceedings of the 2018 AIAA/CEAS Aeroacoustics Conference*, June 25–29, Atlanta, GA, AIAA Paper 2018-3615.
Pineau, P., and Bogey, C. (**2019**). "Steepened Mach waves near supersonic jets: Study of azimuthal structure and generation process using conditional averages," J. Fluid Mech. **880**, 594–619.
Pineau, P., and Bogey, C. (**2020**). "Temperature effects on convection speed and steepened waves of temporally developing supersonic jets," AIAA J. **58**(3), 1227–1239.
Reichman, B. O., Gee, K. L., Neilsen, T. B., and Miller, K. G. (**2016**). "Quantitative analysis of a frequency-domain nonlinearity indicator," J. Acoust. Soc. Am. **139**(5), 2505–2513.
Rossmann, T., Mungal, M. G., and Hanson, R. K. (**2002**). "Evolution and growth of large-scale structures in high compressibility mixing layers," J. Turbul. **3**, N9.
Sabatini, R., Marsden, O., Bailly, C., and Bogey, C. (**2016**). "A numerical study of nonlinear infrasound propagation in a windy atmosphere," J. Acoust. Soc. Am. **140**(1), 641–656.
Saxena, S., Morris, P. J., and Viswanathan, K. (**2009**). "Algorithm for the nonlinear propagation of broadband jet noise," AIAA J. **47**(1), 186–194.
Schlinker, R. H., Liljenberg, S. A., Polak, D. R., Post, K. A., Chipman, C. T., and Stern, A. M. (**2007**). "Supersonic Jet Noise Characteristics & Propagation: Engine and Model Scale," *Proceedings of the 13th AIAA/CEAS Aeroacoustics Conference (28th AIAA Aeroacoustics Conference)*, May 21–23, Rome, Italy, AIAA Paper 2007-3623.
Shepherd, M. R., Gee, K. L., and Wochner, M. S. (**2009**). "Short-range shock formation and coalescence in numerical simulation of broadband noise propagation," J. Acoust. Soc. Am. **126**(6), 2886–2893.
Tam, C. K. W. (**1995**). "Supersonic jet noise," Annu. Rev. Fluid Mech. **27**(1), 17–43.
Tam, C. K. W., Spyropoulos, J. T., Aubert, A. C., and Powers, R. W. (**2018**). "Crackle in the noise of high-performance aircraft," *Proceedings of the 2018 AIAA/CEAS Aeroacoustics Conference*, June 25–29, Atlanta, GA, AIAA Paper 2018-3306.
Tam, C. K. W., and Dong, Z. (**1996**). "Radiation and outflow boundary conditions for direct computation of acoustic and flow disturbances in a nonuniform mean flow," J. Comput. Acoust. **04**(02), 175–201.
Troutt, T. R., and McLaughlin, D. K. (**1982**). "Experiments on the flow and acoustic properties of a moderate-Reynolds-number supersonic jet," J. Fluid Mech. **116**, 123–156.
Whitham, G. B. (**1974**). Linear *N*onlinear *W*aves (Wiley, New York), Chap. 9, pp. 312–338.